1-1-2009

Hydrothermal synthesis and optical, magnetic and supercapacitance properties of nanoporous cobalt oxide nanorodes

Guoxiu Wang
University of Wollongong, gwang@uow.edu.au

Xiaoping Shen
University of Wollongong, xshen@uow.edu.au

Josip Horvat
University of Wollongong, jhorvat@uow.edu.au

Bei Wang
University of Wollongong, bw518@uow.edu.au

Hao Liu
University of Wollongong, hl983@uow.edu.au

See next page for additional authors

Hydrothermal Synthesis and Optical, Magnetic, and Supercapacitance Properties of Nanoporous Cobalt Oxide Nanorods

Guoxiu Wang,*,† Xiaoping Shen,†,‡ Josip Horvat,† Bei Wang,† Hao Liu,† David Wexler,† and Jane Yao†

Institute for Superconducting & Electronic Materials, School of Mechanical, Materials and Mechatronics Engineering, University of Wollongong, NSW 2522, Australia, and School of Chemistry and Chemical Engineering, Jiangsu University, Zhenjiang 212000, China

Received: December 2, 2008; Revised Manuscript Received: January 28, 2009

Nanoporous cobalt oxide nanorods were synthesized by a hydrothermal method. Transmission electron microscopy analysis showed that the individual Co_3O_4 nanorods have a nanoporous structure, consisting of the textured aggregations of nanocrystals. Optical properties of Co_3O_4 nanorods were characterized by Raman and UV−vis spectroscopy. Magnetic property measurement shows that Co_3O_4 nanorods have a low Néel transition temperature of 35 K. We observed quite significant exchange bias for nanoporous Co_3O_4 nanorods, indicating the existence of magnetic coupling between the nanocrystals in Co_3O_4 nanorods. When applied as electrode materials in supercapacitors, Co_3O_4 demonstrated a high capacitance of 280 F/g.

1. Introduction

One-dimensional (1D) nanostructures, including nanowires, nanorods, nanotubes, and nanoribbons, have been extensively investigated in the past few years, mainly due to their peculiar chemical and physical properties. These 1D nanostructures have many technological applications, ranging from as building blocks for fabricating nanoscale electronics and photonics,[1−4] molecular chemical and biological nanosensors,[5,6] to energy storage and conversion.[7]

Cobalt(II,III) oxide (Co_3O_4) with a spinel crystal structure (*Fd*3*m*) has many functional applications, including as heterogeneous catalysts,[8] solid-state sensors,[9] electrochromic devices,[10] solar energy absorbers,[11] and magnetic materials.[12] In particular, 1D Co_3O_4 nanowires and nanotubes have attracted wide interest. Mesoporous Co_3O_4 nanowire arrays have been prepared by a facile solution-based synthesis route.[13] Polycrystalline Co_3O_4 and Au−Co_3O_4 nanowires have been synthesized by virus-enabled assembly and exhibited a high lithium storage capacity.[14] Needlelike Co_3O_4 nanotubes were also prepared via a self-supported formation process, which demonstrated high capacity with improved cycle life and high rate capability in lithium ion cells.[15] Nanocast Co_3O_4 nanowires show a unidirectional exchange anisotropy with an enhancement of the field-cooled coercivity at low temperature.[16]

Herein, we report the effective synthesis of nanoporous Co_3O_4 nanorods by a hydrothermal method. The crystal structure, optical, magnetic, and supercapacitance properties of Co_3O_4 nanotubes were examined by transmission electron microscopy (TEM), ultraviolet−visible (UV−vis) spectroscopy, Raman spectroscopy, magnetic measurements, and electrochemical testing. Nanoporous Co_3O_4 nanorods exhibited unusual magnetic behavior related to surface spins and a high supercapacitance when used as an electrode material in supercapacitors.

* Corresponding author. E-mail: gwang@uow.edu.au. Phone: 61-2-42215726. Fax: 61-2-42215731.
† University of Wollongong.
‡ Jiangsu University.

2. Experimental Section

Materials Synthesis. All chemicals were analytical grade reagent purchased from Sigma-Aldrich. In a typical synthesis of Co_3O_4 nanorods, 1.2 g of cobalt chloride ($CoCl_2$) and 0.06 g of urea ($CO(NH_2)_2$) were dissolved in 20 mL of distilled water to form homogeneous solutions, respectively. The urea solution was then added dropwise to the $CoCl_2$ solution with stirring. The mixture was then transferred to a 50 mL Teflon-liner autoclave, which was sealed and heated to 105 °C for 6 h. After the autoclave was cooled to room temperature, the resulting pink precipitate was separated by centrifugation, washed three times with distilled water and ethanol, respectively, and dried in a vacuum oven. The dried product was then sintered at 300 °C for 3 h. The final black powders were then obtained.

Materials Characterization. The phase identity of the as-prepared product was characterized by X-ray diffraction (XRD, Cu Kα radiation, Philips 1730 diffractometer). The morphology and crystal structure of Co_3O_4 nanorods were analyzed by transmission electron microscope (TEM, JEOL 2011) and high resolution TEM (HRTEM). The specific surface area of the Co_3O_4 nanorods was measured by the gas adsorption technique, using a Quanta Chrome Nova 1000 Gas Sorption Analyzer based on the Brunauer−Emmett−Teller (BET) method. The optical properties of the Co_3O_4 nanorods were characterized by Raman spectroscopy and UV−vis spectroscopy. Raman spectra of the Co_3O_4 nanorods were collected with a Jobin Yvon HR800 confocal Raman system with 632.8 nm diode laser excitation on a 300 lines/mm grating at room temperature. The band gap of the Co_3O_4 nanorods was determined by UV−vis spectroscopy, using a Shimadzu 1700 UV−vis spectrometer.

Magnetic Property Measurement. Magnetic properties of Co_3O_4 nanorods were measured by using the extraction magnetometer in a Quantum Design Physical Properties Measurement System (PPMS). The magnetic moment was measured as a function of temperature under zero-field cooled (ZFC) and field-cooled (FC) conditions. In ZFC measurements, the sample was cooled from room temperature to 5 K in Earth's field. At 5 K, a field of 1 T was applied and magnetization was recorded

10.1021/jp8106149 CCC: $40.75
Published on Web 02/20/2009

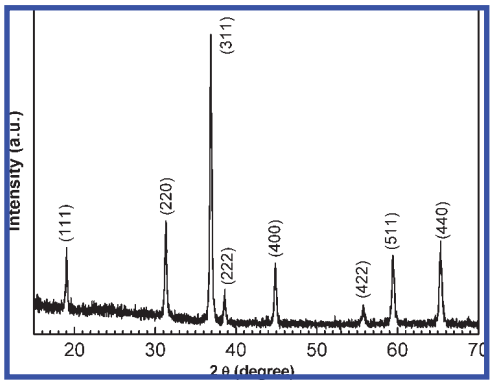

Figure 1. X-ray diffraction pattern of Co_3O_4 nanorods.

upon warming to room temperature. In FC measurements, the sample was cooled from room temperature to 5 K in a field of 1 T. The sweep rate of the temperature was 1.5 deg/min, resulting in no apparent temperature lag between the sample and thermometer, and therefore no discernible difference in the magnetic moment at high temperatures for the ZFC and FC regimes. Measurements of magnetic hysteresis loops were performed at 5, 100, and 200 K with fields up to 7 T. The sweep rate of the field was 50 Oe/s.

Supercapacitance Testing. A beaker-type three-electrode cell was fabricated utilizing Co_3O_4 nanorods with carbon black and polyvinylidene difluoride (PVdF) as the working electrode. Co_3O_4 nanorods (63.5 wt %), carbon black (27.0 wt %), and PVdF binder (9.5 wt %) were ground thoroughly and dispersed in *N*-methyl-2-pyrrolidinone (NMP) solvent to form a slurry. Then the slurry was spread onto a piece of platinum foil and maintained at 120 °C in a vacuum oven overnight. Platinum foil and a saturated calomel reference electrode (SCE) were used as the counter electrode and the reference electrode, respectively. The electrochemical properties were evaluated in 2 M KOH electrolyte at room temperature by the cyclic voltammetry (CV) method on an Electrochemical Workstation (CHI 660C). CV measurements were conducted over the voltage range from −0.25 to 0.55 V at various scan rates (5, 10, 20, 50, and 100 mV s^{-1}). Cycling tests were performed in the same voltage range, with a scan rate of 100 mV s^{-1} for 1000 cycles.

3. Results and Discussion

The phase identity of the as-prepared Co_3O_4 nanorods was determined by X-ray diffraction. Figure 1 shows the XRD pattern of the Co_3O_4 nanorods. All diffraction lines can be indexed to a cubic phase (SG: *Fd*3*m*), confirming the pure phase of the product. The morphology and crystal structure of Co_3O_4

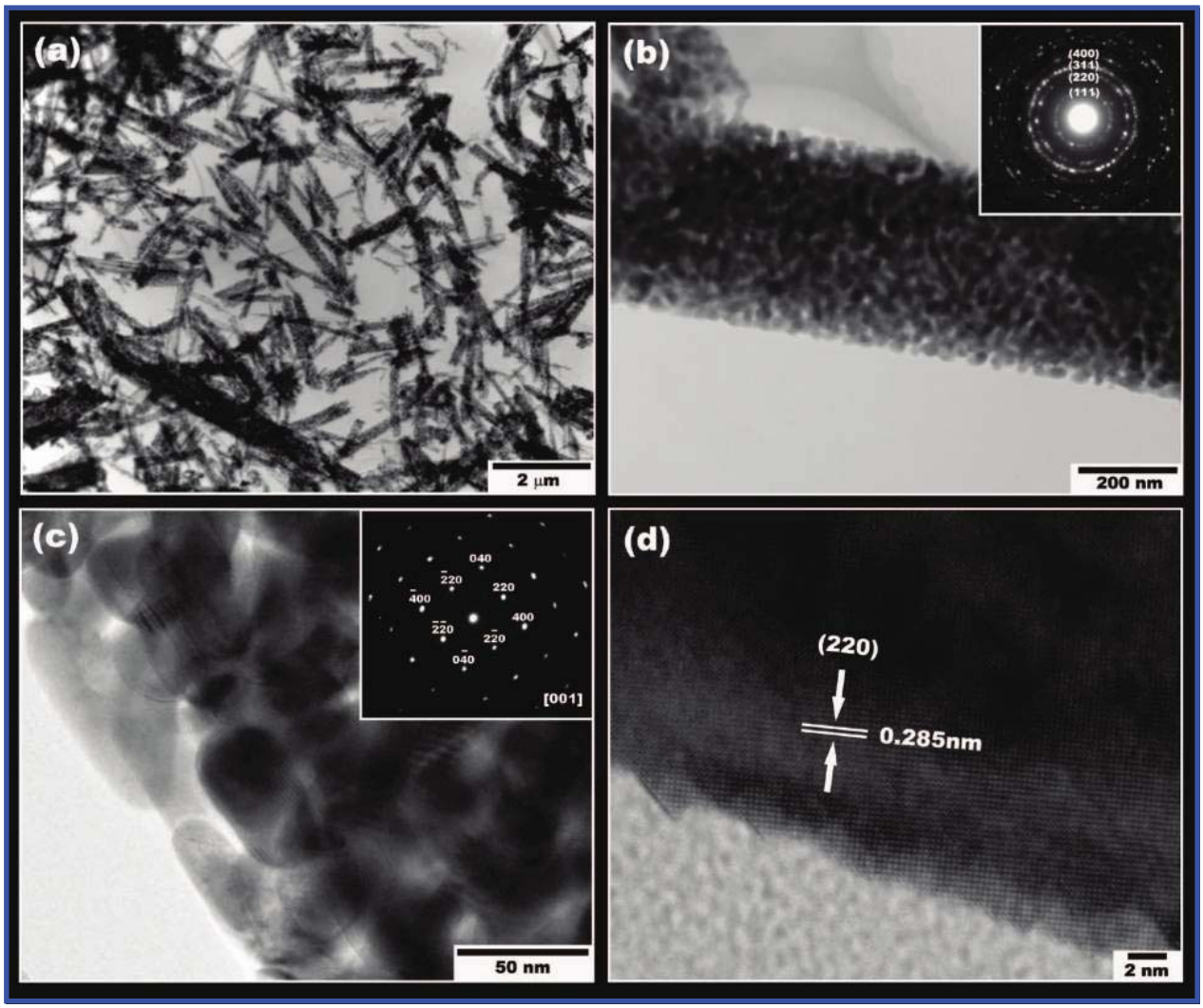

Figure 2. (a) Low magnification TEM image of Co_3O_4 nanorods. (b) High magnification TEM image of a single Co_3O_4 nanorod, showing the porous structure. The inset is the corresponding electron diffraction pattern. (c) HRTEM image of part of a single Co_3O_4 nanorod, from which the crystal size and pore size can be determined. In inset is the selected area electron diffraction pattern obtained by converge beam. (d) Lattice resolved HRTEM image of a single Co_3O_4 nanocrystal.

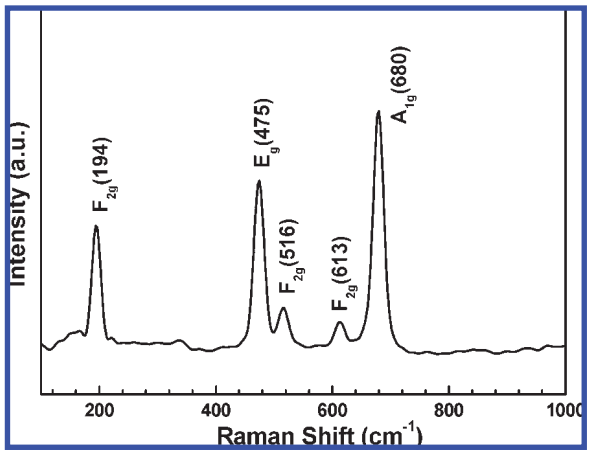

Figure 3. Room temperature Raman spectrum of Co_3O_4 nanorods.

nanorods were analyzed by TEM and HRTEM analysis. Figure 1a shows a general low magnification bright-field TEM image of the as-prepared Co_3O_4 nanorods. The lengths of nanorods extend a few micrometers. A high magnification TEM image of a single Co_3O_4 nanorod is shown in Figure 1b, from which the diameter of the nanorods was determined to be about 400 nm. It is clearly visible that the Co_3O_4 nanorod is polycrystalline and has a nanoporous structure. The porous Co_3O_4 nanorods could be formed via two steps. In the first step, the nanorods of the intermediate product $Co^{II}(OH)_a(CO_3)_bCl_{(2-a-2b)}\cdot nH_2O$ was formed in the hrdrothermal process. In the second step, those precursors were converted into porous Co_3O_4 nanorods in the calcination process. As revealed by Zou et al.,[17] the crystal structure of $Co^{II}(OH)_a(CO_3)_bCl_{(2-a-2b)}\cdot nH_2O$ includes Co−OH layers and counteranions between the Co−OH layers. During the sintering process, the Co−OH layers are converted into cobalt oxide nanoparticles through the dehydration and pyrolysis of counteranions into gases (such as CO_2 and HCl). The spaces of the −OH and counterions are converted into nanopores. Selected area electron diffraction (SAED) was performed on the nanorods, and the SAED pattern is shown as the inset in Figure 2b. The diffraction rings can be fully indexed to the cubic Co_3O_4 crystal structure. Figure 2c shows a high resolution TEM image of part of a Co_3O_4 nanorod. The individual nanocrystals have a shape resembling elongated elipses, with a size in the range of 20−30 nm. We can also identify that the pore sizes are in the range of a few nanometers. We performed the SAED on the region shown in Figure 2c along the [001] zone axis. A spot SAED pattern was obtained and is shown as the inset in Figure 2c, indicating that the Co_3O_4 nanocrystals grew along one direction and aggregated into a porous structure. The lattice resolved HRTEM image of part of a Co_3O_4 nanocrystal is shown in Figure 2d. The interplanar spacing was measured to be 0.285 nm, corresponding to the (220) crystal planes. The specific surface area of the Co_3O_4 nanorods was measured to be 232 $m^2\ g^{-1}$ (BET area), which is much higher than that of the commercial microcrystalline Co_3O_4 powders (7 $m^2\ g^{-1}$).

The optical properties of the Co_3O_4 nanorods were characterized by Raman spectroscopy and UV−vis spectroscopy. Figure 3 shows the Raman spectrum of the Co_3O_4 nanorods. Five distinguishable Raman peaks are located at 194, 475, 516, 613, and 680 cm^{-1}, respectively. They correspond to 3 $F_{2\ g}$, 1 E_g, and 1 $A_{1\ g}$ Raman active modes of the Co_3O_4 nanocrystals, as labeled in Figure 3. The phonon symmetries of the Raman peaks are caused by the lattice vibrations of the spinel structure, in which Co^{2+} and Co^{3+} cations are situated at tetrahedral and octahedral sites in the cubic lattice. The frequencies of all the

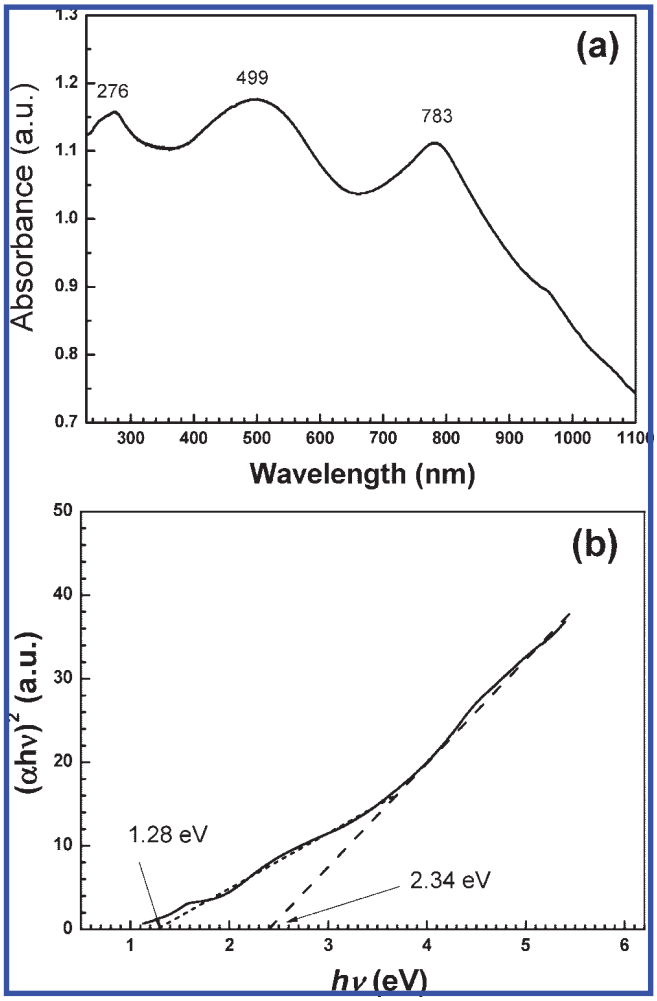

Figure 4. (a) UV−vis absorbance spectrum of Co_3O_4 nanorods. (b) Optical band gap energy of Co_3O_4 nanorods obtained by extrapolation to $\alpha = 0$.

Raman peaks of Co_3O_4 nanorods are similar to theose standard microcrystalline Co_3O_4 powders.[18]

Co_3O_4 is a *p*-type semiconductor. The optical band gap of Co_3O_4 is strongly influenced by the size, shape, and dimensions of materials. Figure 4a shows the UV−vis absorbance spectrum of the Co_3O_4 nanorods. The band gap E_g can be calculated from the equation:

$$(\alpha h\nu)^n = B(h\nu - E_g) \quad (1)$$

where α is the absorption coefficient, $h\nu$ is the photon energy, B is a constant characteristic to the material, and n equals either 1/2 for an indirect transition, or 2 for a direct transition. The $(\alpha h\nu)^2$ versus hν curve is shown in Figure 4b. The value of $h\nu$ extrapolated to $\alpha = 0$ gives the absorption band gap energy. The curve in Figure 4b can be linearly fitted into 2 lines with the intercepts at 1.28 and 2.34 eV, respectively. The band gap of 2.34 eV should be associated with the $O^{2-} \rightarrow Co^{2+}$ charge transfer process (valence to conduction band excitation), while the band gap of 1.28 eV can be assigned to $O^{2-} \rightarrow Co^{3+}$ charge transfer (with the Co^{3+} level located below the conduction band). The best fit of eq 1 gives $n = 2$, suggesting that the obtained Co_3O_4 nanorods are semiconducting with a direct transition.[19,20]

The magnetic response of the Co_3O_4 nanorods should be the result of the complex interaction between the individual Co_3O_4 nanocrystals and the collective magnetic properties of the

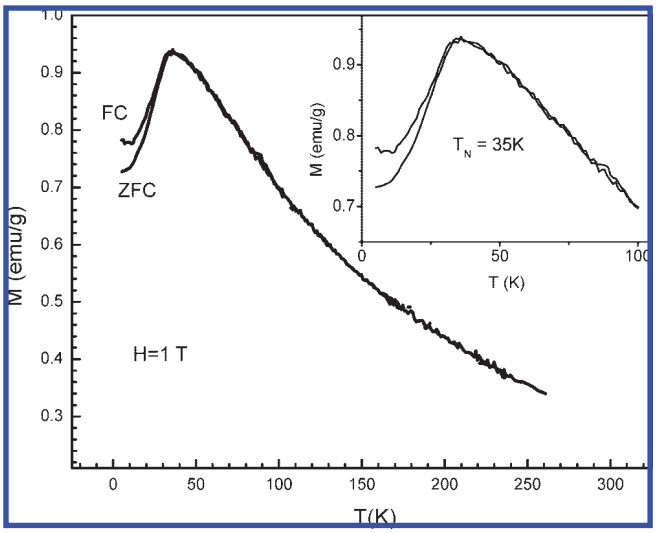

Figure 5. Temperature dependence of zero-field-cooled (ZFC) and field-cooled (FC) magnetic moment of Co_3O_4 nanorods, measured in the field of 1 T. Inset: Details below 100 K, showing Néel temperature of 35 K.

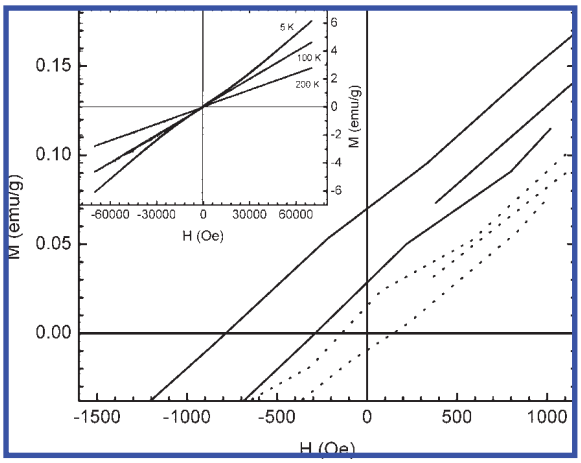

Figure 6. Magnetic hysteresis loops of Co_3O_4 nanorods measured at 5, 100, and 200 K. The main figure shows the details around zero field for the hysteresis loops measured at 5 (solid line) and 100 K (dashed line).

nanorods. The influence of the shape anisotropy of the nanorods can be excluded because the sample powders consist of randomly oriented Co_3O_4 nanorods. The temperature dependence of the magnetic moment of the Co_3O_4 nanorods is shown in Figure 5, the data for which were collected under ZFC and FC conditions. The ZFC and FC points overlap above 35 K, showing a paramagnetic response. The inset in Figure 5 shows more details of ZFC and FC measurements below 100 K. There is a cusp at $T = 35$ K for both ZFC and FC magnetization, which corresponds to the Néel transition. The ZFC and FC magnetic measurements were also performed with the field of $H = 300$ Oe. The results of the cusp at 35 K and a difference between ZFC and FC measurements below 35 K are qualitatively the same as those for $H = 1$ T. We interpret this cusp as an antiferromagnetic transition for Co_3O_4 nanorods at 35 K. ZFC and FC magnetic moments show no overlap below 35 K, and there also exists an increase of magnetic moment with decrease of temperature for FC measurement below 10 K.

Because Co_3O_4 nanorods consist of nanocrystals with a size of about 30 nm, which are ordered into a porous nanorod shape, there is the possibility that there are unpaired spins near the surface of the nanocrystals which do not have an antiferromagnetically coupled counterpart. This would result in a substantial nonzero magnetic moment of the sample, because the surface-to-volume ratio of nanocrystals is much larger than that for macroscopic particles. When magnetic field is applied, these unpaired spins would contribute to a substantial magnetic moment of the sample. Their alignment would be disturbed by thermal excitations, resulting in an increase in the magnetic moment with decreasing temperature. However, unpaired spins would be frozen-in at low temperature in the direction of the magnetic field, giving an almost constant magnetic moment at low temperatures in the FC regime. This result was obtained by Salabas et al. for Co_3O_4 nanowires with a diameter of 8 nm.[16] Salabas et al. obtained an increase in the magnetic moment when they cooled their samples through the freezing temperature of 30 K, followed by an almost constant moment at lower temperature in the FC regime. Nethravathi et al. reported a strong increase in the magnetic moment with cooling below 20 K for ZFC and FC measurements in low (50 Oe) and high (5000 Oe) fields on Co_3O_4 nanoparticles with a size of 35 nm.[21] This was explained by a strong interaction between the agglomerated nanocrystals. Our results differ from these in that our FC measurements exhibit a cusp similar to the one for ZFC measurements and show no constant magnetic moment at low temperatures. However, they do not show any evidence of a spin-freezing type of behavior in FC measurements. Therefore, the dominant process in our ZFC and FC measurements could be the antiferromagnetic ordering of Co^{2+} ions.

The obtained value of the Néel temperature, T_N, is below the Néel temperature of 40 K for macroscopic Co_3O_4 crystals.[22,23] This lowering of T_N is due to the geometric confinement effect on the magnetic ordering, which has been shown to reduce the ordering temperature by[24]

$$\Delta T_N = T_{N0}\left(\frac{\xi_0}{d}\right)^{\lambda} \quad (2)$$

where T_{N0}, ξ_0, λ, and d are the Néel temperature for an infinite crystal, the correlation length of the magnetic ordering, the shift exponent, and the size of the nanoparticle, respectively. Values of $\lambda = 1.1$ and $\xi_0 = 2.8$ nm were reported for Co_3O_4 nanoparticles.[25] Because ΔT_N for our sample is 5 K, the size of the particles is expected to be $d = 27$ nm. This is in good agreement with the size of nanocrystals in our nanorods observed from TEM analysis (Figure 2). Our ZFC and FC measurements are in good agreement with the results presented in ref 24, including the increase in the moment with decreasing temperature for $T < 10$ K.

Figure 6 shows the magnetization dependence on the applied magnetic field (hystersis loops) recorded at $T = 5$, 100, and 200 K. The inset in Figure 6 shows magnetic hysteresis loops up to 7 T. There is no apparent hysteresis visible. However, zooming-in around zero field reveals several effects. There are small hysteresis loops for all temperatures and the coercive field decreases with temperature. While all hysteresis loops at $T >$ 35 K are centered on $H = 0$, those for $T < 35$ are shifted to lower values of H. The coercive field at 5 K is 250 Oe and the center of the loop is at $H = -530$ Oe. This loop was measured after field cooling through T_N in a field of 1 T. The coercive fields for hysteresis loops at 100 and 200 K, centered at $H = 0$, are 140 and 90 Oe, respectively. This is consistent with the existence of unpaired spins on the surface of the nanocrystals. Below T_N, there is an exchange bias interaction between ferromagnet-like coupled surface spins and underlying antifer-

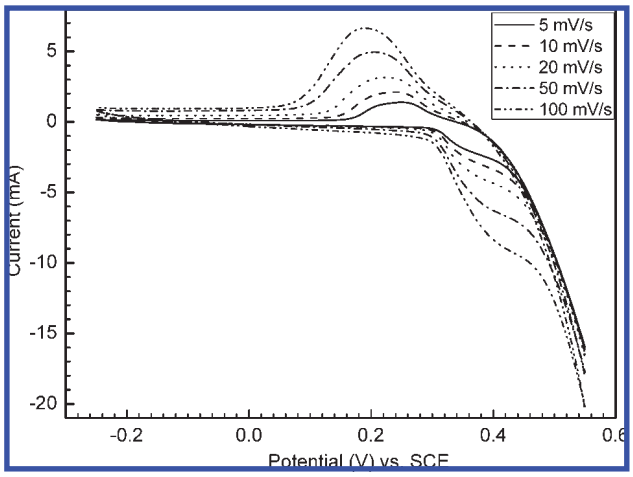

Figure 7. Cyclic voltammograms of Co_3O_4 nanorods as electrode material for supercapacitor application at different scanning rates, from which the capacitance can be calculated.

romagnetically coupled spins, resulting in a shift of the hysteresis loop to negative *H*.

Exchange bias was also reported for Co_3O_4 nanocast nanowires consisting of nanocrystals of 8 nm.[16] Our measurements also support the assumption that the surface spins exhibit a spin-glass-like behavior, resulting in open hysteresis loops at high fields. Therefore, our results for the nanorods made up of ~30 nm nanocrystals are in agreement with the exchange coupling and spin-glass-type behavior also observed in nanowires consisting of 8 nm nanocrystals.[16] This indicates that there is magnetic interaction between the nanocrystals in the nanorods.

However, the results of our ZFC and FC measurements are also quite different than those of the nanocast nanowires, lacking any evidence for spin freezing. Instead, our ZFC and FC measurements closely resemble the ones obtained for nanoparticles between 16 and 75 nm in diameter.[23] Our nanorods were too large to exhibit superparamagnetism, as was observed for Co_3O_4 nanoparticles 3 nm in diameter.[26] Coupling between the nanocrystals in the nanorods would also impede superparamagnetic behavior. Therefore, our samples fall in between those that exhibit strong interaction between the nanocrystals, resulting in suppression of superparamagnetism and a ferromagnetic-like spin glass and those that exhibit no coupling between nanoparticles, resulting in the absence of exchange bias.[27]

Supercapacitance of the Co_3O_4 nanorod electrode was measured via cyclic voltammetry (CV). Figure 7 shows the CV curves at various sweep rates. All CV profiles have similar shapes with reduction and oxidation peaks rather than ideally rectangular shapes. This indicates that the capacitance obtained was not pure double layer capacitance, but mainly originated from faradaic pseudocapacitance. The maximum specific capacitance of 281 F g^{-1} was obtained at a 5 mV s^{-1} scan rate in 2 M KOH solution. As a comparison, commercial microcrystalline Co_3O_4 powders were also tested through the same procedures, giving a maximum specific capacitance value of 43 F g^{-1}. The high supercapacitance of Co_3O_4 nanorods could be attributed to the nanoporous structure of nanorods with high specific surface area.

4. Conclusions

Nanoporous Co_3O_4 nanorods can be effectively synthesized in large quantity through the hydrothermal method. TEM and HRTEM analysis indicated the individual Co_3O_4 nanorods consist of aggregated nanocrystals with a nanoporous structure. The nanoporous Co_3O_4 nanorods exhibited a low Néel temperature of 35 K. Quite significant exchange bias was observed for nanoporous Co_3O_4 nanorods, shifting the magnetic hysteresis loops by −530 Oe at 5 K. The presence of exchange bias indicates the existence of magnetic coupling between the nanocrystals in Co_3O_4 nanorods. Due to the large specific surface area induced by the nanoporous structure, Co_3O_4 nanorods demonstrated a high supercapacitance of 281 F g^{-1}.

Acknowledgment. We are grateful for financial support from the Australian Research Council through the ARC Discovery project (DP0772999).

References and Notes

(1) Duan, X. F.; Huang, Y.; Cui, Y.; Wang, J. F.; Lieber, C. M. *Nature* **2001**, *409*, 66.
(2) Cui, Y.; Lieber, C. M. *Science* **2001**, *291*, 851.
(3) Huang, Y.; Duan, X. F.; Cui, Y.; Lauhon, L.; Kim, K. H.; Lieber, C. M. *Science* **2001**, *294*, 1313.
(4) Pan, Z. W.; Dai, Z. R.; Wang, Z. L. *Science* **2001**, *291*, 1947.
(5) Cui, Y.; We, Q. Q.; Park, H. K.; Lieber, C. M. *Science* **2001**, *293*, 1289.
(6) Yun, M. H.; Myung, N. V.; Vasquez, R. P.; Lee, C.; Menke, E.; Penner, R. M. *Nano Lett.* **2004**, *4*, 419.
(7) Park, M. S.; Wang, G. X.; Kang, Y. M.; Wexler, D.; Dou, S. X.; Liu, H. K. *Angew. Chem., Int. Ed.* **2005**, *46*, 750.
(8) Švegl, F.; Orel, B.; Grabec-Švegl, I.; Kauèiè, V. *Electrochim. Acta* **2000**, *45*, 4359.
(9) Yamaura, H.; Tamaki, J.; Moriya, K.; Miura, N.; Yamazoe, N. *J. Electrochem. Soc.* **1997**, *144*, L158.
(10) Švegl, F.; Orel, B.; Hutchins, M. G.; Kalcher, K. *J. Electrochem. Soc.* **1996**, *143*, 1532.
(11) Hutchins, M. G.; Wright, P. J.; Grebenik, P. D. *Solar Energy Mater.* **1987**, *16*, 113.
(12) Nethravathi, C.; Sen, S.; Ravishankar, N.; Rajamathi, M.; Pietzonka, C.; Harbrecht, B. *J. Phys. Chem. B* **2005**, *109*, 11468.
(13) Li, Y. G.; Tan, B.; Wu, Y. Y. *J. Am. Chem. Soc.* **2006**, *128*, 14258.
(14) Nam, K. T.; Kim, D. W.; Yoo, P. J.; Chiang, C. Y.; Meethong, N.; Hammond, P. T.; Chinag, Y. M.; Belcher, A. M. *Science* **2006**, *312*, 885.
(15) Lou, X. W.; Deng, D.; Lee, J. Y.; Feng, J.; Archer, L. A. *Adv. Mater.* **2008**, *20*, 258.
(16) Salabas, E. L.; Rumplecker, A.; Kleitz, F.; Radu, F.; Schuth, F. *Nano Lett.* **2006**, *6*, 2977.
(17) Hosono, E.; Fujihara, S.; Honma, I.; Zhou, H. S. *J. Mater. Chem.* **2005**, *15*, 1938.
(18) Hadjiev, V. G.; Iliev, M. N.; Vergilov, I. V. *J. Phys. C: Solid State Phys.* **1998**, *21*, L199.
(19) Barreca, D.; Massignan, C.; Daolio, S.; Fabrizio, M.; Piccirillo, C.; Armelao, L.; Tondello, E. *Chem. Mater.* **2001**, *13*, 588.
(20) Xu, R.; Zeng, H. C. *Langmuir* **2004**, *20*, 9780.
(21) Nethravathi, C.; Sen, S.; Ravishankar, N.; Rajamathi; Pietzonka, C.; Harbrecht, B. *J. Phys. Chem. B* **2005**, *109*, 11468.
(22) Roth, W. L. *J. Phys. Chem. Solids* **1963**, *25*, 1.
(23) Spencer, C. D.; Schroeer, D. *Phys. Rev. B* **1974**, *9*, 3658.
(24) Ambrose, T.; Chien, C. L. *Phys. Rev. Lett.* **1996**, *76*, 1743.
(25) He, L.; Chen, C.; Wang, N.; Zhou, W.; Guo, L. *J. Appl. Phys.* **2007**, *102*, 103911.
(26) Meiklejo, W. H. C. P.; Bean, C. P. *Phys. Rev.* **1956**, *102*, 1413.
(27) Takada, S.; Fujii, M.; Kohiki, S.; Babasaki, T.; Deguchi, H.; Mitome, M.; Oku, M. *Nano Lett.* **2001**, *1*, 379.

JP8106149